Elastic collisions of low- to intermediate-energy electrons from carbon dioxide: Experimental and theoretical differential cross sections

H. Tanaka,* T. Ishikawa, T. Masai, T. Sagara, and L. Boesten
Department of Physics, Sophia University, Tokyo 102, Japan

M. Takekawa and Y. Itikawa
Institute of Space and Astronautical Science, Sagamihara, Kanagawa 229, Japan

M. Kimura
School of Allied Health Sciences, Yamaguchi University, Ube, Yamaguchi 755, Japan
and Department of Physics, Rice University, Houston, Texas 77251
(Received 17 January 1997; revised manuscript received 12 May 1997)

Absolute elastic differential cross sections for electron collision with carbon dioxide (CO_2) at impact energies from 1.5 to 100 eV and scattering angles from 15° to 130° have been measured. Also, a calculation has been made that uses two different types of close-coupling approaches and covers all scattering angles in the same energy region. The measurements are in excellent agreement with observations by other authors. They also agree with the present calculation for all energies above 10 eV. The agreement becomes less satisfactory as the energy decreases below 8 eV, particularly at scattering angles below 60°, where the measurements show a conspicuous shoulder around this angle in the energy between 5 and 7 eV. Integral and momentum-transfer cross sections have been estimated from extrapolations to 0° and 180°. Extensive comparisons with recent other theories are included. [S1050-2947(98)07702-6]

PACS number(s): 34.10.+x, 34.80.−i

I. INTRODUCTION

Due to its importance in applied fields from astrophysics and aeronomy to plasma chemistry, carbon dioxide (CO_2) remains one of the most popular molecules for a test study of electron scattering [1]. Earlier, Itikawa and Shimizu [2] compiled a set of cross sections of electron scattering from CO_2 for a variety of elastic and inelastic processes over a wide range of collision energies by collecting and critically examining all published data at that time, and the data they reported have been widely used for applications, particularly in astrophysics and radiation physics.

Since then, there have been a number of experimental and theoretical studies both for elastic and inelastic (mostly for vibrational excitation and limited numbers of electronic excitation) processes. Shyn, Sharp, and Carignan [3] measured elastic scattering and obtained the total and differential cross sections DCS's in the energy of 3–90 eV. Register, Nishimura, and Trajmar [4] carried out a measurement of the absolute cross sections at 4, 10, 20, and 50 eV. Kanik, McCollum, and Nickel [5] obtained the differential cross sections for scattering angles between 20°–120° at 20–100 eV energies. Iga, Nogueira, and Lee [6] measured the absolute elastic cross sections at 500, 800, and 1000 eV. More recently, Nakamura [7] made a swarm experiment to determine a new set of cross sections including momentum transfer.

Theoretically, Morrison, Lane, and Collins [8] studied the elastic process by using a close-coupling scheme for collision energies from 0.07 to 10 eV. In their treatment, the polarization potential was determined semiempirically. Lucchese and McKoy [9] calculated the elastic cross sections based on the Schwinger variational method with neglect of the correlation polarization potential for collision energies between 0.1 and 13.6 eV. Truhlar and co-workers [10] performed a theoretical study for energies of 10 and 20 eV that is based on semiempirically determined molecular wave functions for the target molecule and on a separate treatment of the correlation polarization potential with an adjustable parameter. Botelho *et al.* [11] adopted a rather crude approximation by using, as a long-range force, only the spherical polarization potential and neglecting exchange interaction, and calculated elastic cross section for 20–1500 eV region. Very recently Takekawa and Itikawa [12] made a theoretical study of elastic scattering of electrons from CO_2. Their calculation was based on an *ab initio* self-consistent-field (SCF) wave function of the target molecule. They solved the close-coupling equations in the fixed-nuclei approximation, and took into account the effects of electron exchange and target polarization with the help of local model potentials. They compared their DCS's for 10–50 eV with the experiments of Refs. [4] and [5]. In addition to this recent study, Gianturco and Stoecklin [13], and Gianturco and Lucchese [14] calculated the elastic cross sections based on a close-coupling scheme in the energy region from 0.02 to 100 eV.

Although remarkable progress has been made both in the experimental and theoretical approaches for electron scattering from CO_2 molecules, unfortunately, there still remain a few problems to be resolved: (i) too little is known to form a complete and comprehensive set of data of absolute experimental DCS's for elastic and inelastic processes; (ii) the agreement between the various experiments as well as between theory and experiment is yet unsatisfactory for practi-

*Electron mail address: h_tanaka@hoffman.cc.sophia.ac.jp

 © 1998 The American Physical Society

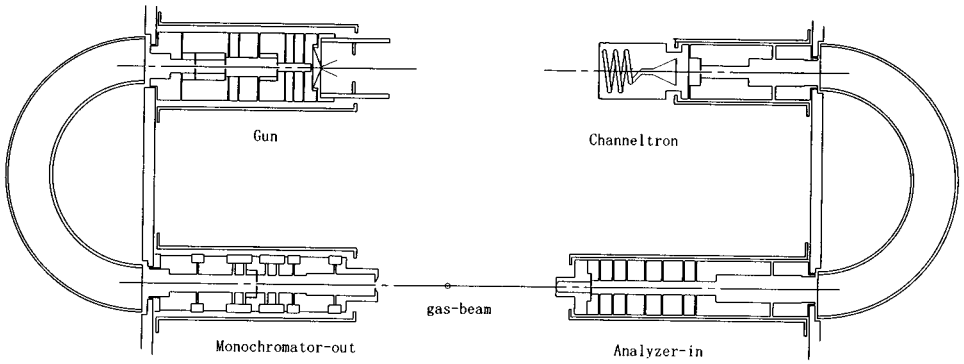

FIG. 1. Top view of the spectrometer (true to scale).

cal purposes, especially at low energies; and (iii) little detailed quantitative information is available on both the differential and integral cross sections in the resonance region, although its position has been confirmed reasonably well by experiments.

We have conducted a joint experimental and theoretical study to determine the differential and integrated cross sections for elastic processes in collisions of electrons with CO_2 for incident energies from 1.5 to 100 eV. In the present paper, the calculation by Takekawa and Itikawa [12] is extended to energies as low as 1.5 eV and as high as 100 eV. The previous study suggested that the theoretical result may become more sensitive to the interaction potential adopted in the energy region below 10 eV. Hence another type of calculation was added for the lower-energy region. In that calculation, a multiconfiguration self-consistent-field (MC-SCF) wave function is used for the target, and a slightly different model is adopted for the local exchange and polarization potentials. In the following, the newly obtained set of experimental cross sections is compared with the two different sets of theoretical cross sections to provide a comprehensive set of elastic cross sections for CO_2.

II. EXPERIMENTAL TECHNIQUES

A. General setup

The spectrometer is a crossed-beam apparatus with single hemispherical energy selectors of mean radius 42 mm and a pass energy of 1.5–2 eV with virtual entrance and exit apertures (see Fig. 1). Cylindrical lenses are used throughout. All apertures and lens elements are made of molybdenum. Overall resolution at Faraday-cup currents of 5–9 nA was about 33 meV (full width at half maximum of the observed elastic peaks), sufficient to separate the elastic peak from vibrational excitations, but not from rotational excitations. In the following, we simply call the vibrationally elastic cross sections elastic cross sections. The background pressure in the vacuum chamber is about 3×10^{-6} torr with the gas beam turned on. A combination of a 2-mm-thick μ-metal shield with Helmholtz coils around the top and bottom flanges of the vacuum vessel reduce the earth's magnetic field to less than 5 mG. The angular resolution amounts to about $\pm2°$. Variations of the electron-beam intensity with different gases are reduced by enclosing the electron-beam generating system and the analyzer in separate casings and pumping them differentially. The nozzle (a simple molybdenum tube of diameter 0.3 mm and length 5 mm) was kept at 50 °C above room temperature to prevent accumulation of surface charges. We did not observe any effects of CO_2 on our thoriated iridium filament [5].

B. Relative flow method

The relative flow method was developed at the Jet Propulsion Laboratory of the California Institute of Technology [4,15–17]. It bypasses the determination of many experimental parameters required for an absolute measurement of the cross sections by comparing the measurements of the gas (g) under study with those of a reference gas (r) of known DCS's under identical experimental conditions except for the flow rates, i.e., the backing pressures at the nozzle entrance. However, a few details have to be attended to carefully. When the flow rates are adjusted according to

$$\frac{N_g'}{N_r'}=\frac{\sigma_r^2}{\sigma_g^2}\left(\frac{M_r}{M_g}\right)^{1/2}, \tag{1}$$

the mean free path lengths at the entrance of the nozzle and consequently the angular distribution of the two gases emanating from the nozzle remain nearly constant as long as a loosely defined upper limit for the pressure is observed [15,17]. Here σ is the collisional diameter of the gas, M the molecular mass, and N' the flow rate. Under these conditions the DCS (Σ) of the gas under investigation can be calculated from the well-known formula

$$\frac{\Sigma_g}{\Sigma_F}=\frac{I_g}{I_r}\left(\frac{M_r}{M_g}\right)^{1/2}\frac{N_r'}{N_g'}, \tag{2}$$

where I refers to the scattered electron counts per sweep and $N'\sqrt{M}=F$ is the normalized flow rate that would be proportional to the backing pressure P for an ideal gas. However, there have been persistent reports of a nonlinear relation between normalized flow-rates and backing pressures [18–22]. They often refer to nozzle arrays with narrow capillary diameters (e.g., 0.05 mm [18]) and show plots of F vs P that deviate from the low-pressure, straight line through the origin by 7.7% [23], 9.1% [20], and 9.8% [21] to 28.6% [19]. We have therefore calibrated our flow rates as follows, cf. Fig. 2, where we refer to one arm of the piping from the reduction valve of the gas cylinder (not shown) to the nozzle with all irrelevant valves closed. The initial pressure increase after suddenly opening the needle valve in the fixed volume $V=V_g=V_r$ between leak valves and nozzle (piping plus capacitance manometer, a Baratron) is recorded while gas is

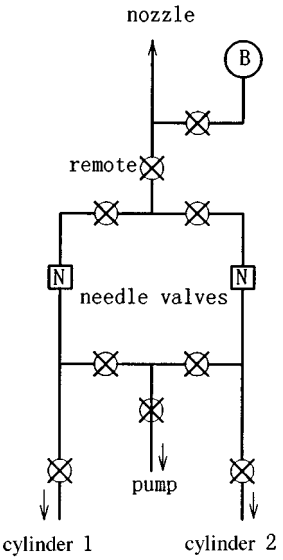

FIG. 2. Gas handling system. *N* are needle valves, *B* is a capacitance manometer (Baratron).

allowed to simultaneously ''leak'' out of the nozzle; for sample plots; see, e.g., Ref. [22]. The process can be described by differentiating the ideal gas formula as

$$V\frac{dP}{dt}=kT\frac{dN}{dt}-P\frac{dV}{dt}. \tag{3}$$

N is the number of molecules, and dV/dt represents the pumping speed of the leak [23]. For a constant pumping speed and constant dN/dt this equation has the general solution

$$P(t)=B+A[1-e^{\beta(t-t_0)}], \tag{4}$$

where B recalibrates the Baratron, A is the (corrected) final pressure, and t_0 compensates for a late start of the observations, thus allowing exclusion of transient pressure fluctuations in the first 10–20 s. The observations extend up to 500 s, and the largest deviation between fit and data beyond 20 s is less than 1.5%. The four parameters of Eq. (4) were obtained by least-square fitting to the $P(t)$ traces observed for the two pressures used in this experiment. B contributes less than 0.5% and is neglected in the following. Then the flow rate $N'=dN/dt$ is proportional to the final pressure, $N'\propto P_\infty\beta$, so that Eq. (2) can be rewritten

$$\frac{\Sigma_g}{\Sigma_r}=\frac{I_g}{I_r}\frac{P_r}{P_g}\frac{\beta_r\sqrt{M_r}}{\beta_g\sqrt{M_g}} \tag{5}$$

where the last factor gives a correction factor γ to the simple pressure formula of Trajmar and Register [18]. For our tube-nozzle of 0.3-mm diameter, and for the gases and the pressures used in these experiments, γ was 0.98, well within the uncertainties of determining the corrections themselves. Our single point evaluation of γ should not be extended to other pressures or other gases.

Reference [24] gives the collision diameters for He and CO_2 as 2.19 and 4.64 Å, respectively. Newer estimates [25] give 2.19 and 4.53 Å, and thus the theoretical pressure ratio for equal Knudsen numbers would be 4.1:1. We used 4 torr for He, and 1 torr for CO_2. The theory of Olander and Kruger [26], also quoted in Refs. [17] and [15], is valid for $\gamma<K_L<10$, where $\gamma=D/L$, $K_L=\lambda/L$, D is the diameter and L the length of the nozzle, and the mean free path λ refers to the reservoir behind the nozzle. This becomes $0.06<0.0074<10$ in our case, with $\lambda=36.8\ \mu$m. Brinkman and Trajman used Knudsen numbers below this limit when comparing their theory with experiment, and we ourselves have directly observed a radial density distribution from a heated nozzle in the form of colorful deposition patterns of C_{60} that differs in shape from those reported in Ref. [27], but can be fitted very well from Olander and Kruger's theory, even at a Knudsen number far below the limits indicated in Olander and Kruger's paper.

C. Transmission function

All lens voltages have been calculated with a computer program [28] that traces electrons through the electric fields of the lenses and minimizes the sum of the squared deviations from user-specified aims like image position, magnification, and beam angle by automatically adjusting three of the lens voltages. Other voltages are set such that the maximum angle (beam angle plus pencil) is less than 5.5° over the full range of residual energies down to 0.5 eV. After calculating a set of variable voltages for 10–15 residual energies, we pass a cubic spline through the data and use the spline to drive the lenses by computer. Such voltage sets have been calculated for all impact energies from 1.5 to 100 eV.

The literature reports variations in the transmission function of the analyzer of 1:5.5 over a residual energy range from 2 to 8.5 eV [15], and proposes an elaborate method for verification. We have checked our analyzer response as follows. The control measurements of He in the relative flow method, repeated for all angles and impact energies, can be interpreted as an attempt to obtain the *relative* DCS of the reference gas. That is, the He counts observed over the full range of energies and normalized (equal to the per sweep–pressure–electron-current), should give a set of DCS's that need only a single scaling factor to obtain the theoretical DCS of He. A constant factor over all residual energies would imply an ideal response of the analyzer, and, conversely, a strongly nonuniform response should show up as a consistent pattern in all plots of the scaling factor as function of residual energies. Two recent samples of such ratios $\Sigma(\mathrm{He}_{\mathrm{meas}})/\Sigma(\mathrm{He}_{\mathrm{theory}})$ for a scattering angle of 90° are shown in Fig. 3. They have been scaled for a nominal factor of 1. We attribute the remaining fluctuations to the difficult and operator-dependent adjustment of the *shape* of electron beam. Standard deviations are 15% and 24%, maximum deviations are 26% and 41%, and all deviations are randomly distributed over more than 20 repetitions for the measurements of various gases. The relative flow method cancels the remaining deviations of Fig. 3 and also those that arise with changing angles (within 1:3) as long as the assumption of constant collision volume is fulfilled.

D. Error estimates

The impact energy scale was calibrated against the $2\,^2S$ resonance of He at 19.367 eV [29] up to ± 10 meV, the

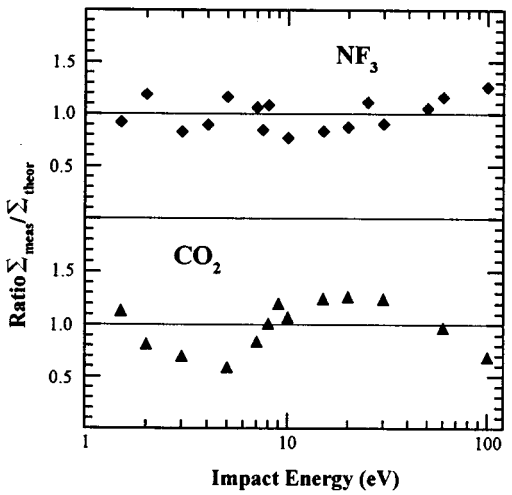

FIG. 3. Samples of the ratio of observed He-DCS to the theoretical He-DCS.

accuracy of all other impact energies depends on a voltage-standard source of claimed accuracy 0.05% up to 100 mA. To increase the effective counts and reduce the dependence on distorted shapes, the counts of the elastic peaks of CO_2 and He are Simpson integrated over ± 30 meV from the peak and entered into Eq. (5). We estimate the error of these measurements as about 10%. The error of the standard He DCS, a smooth fit through many published theoretical and experimental DCS's from 0.1 to 1000 eV, was previously shown to be 10% [30]. The relative pressure readings of the capacitance manometer (MKS Baratron) are claimed to be better than 1%. Uncertainties with the collision volume are hard to estimate. We assume an overall accuracy of about 15% [cf. Ref. [27]]. The background signal at low scattering angles was recorded with the gas beam turned off. It produces a further uncertainty into the 20° DCS to give an overall accuracy of about 20% at the lowest angles.

E. Extrapolation

For comparison with published momentum-transfer cross sections and integrated cross sections, DCS's of the limited angular range have to be extrapolated both at low and high sides of angles. Direct fitting of the DCS's by Legendre polynomials usually fails at higher impact energies because the DCS's drop over decades at low scattering angles and the required higher-order polynomials would then pick up the noise of the experimental data and develop deep wiggles in the extrapolation regions. We therefore use a Legendre-based fitting function derived from inelastic phase-shift fitting of the scattering amplitude,

$$f(\vartheta,k)=\frac{N_k}{2ik}\left[\sum_{\lambda=0}^{L}(2\lambda+1)(\beta_\lambda e^{2i\eta_\lambda}-1)P_\lambda(\cos\vartheta)+f_B^L(\vartheta)\right], \tag{6}$$

$$f_B^L(\vartheta)=-2ik\pi\alpha k\left[\frac{1}{2}\sin\frac{\vartheta}{2}+\sum_{\lambda=0}^{L}\frac{(2\lambda+1)P_\lambda(\cos\vartheta)}{8\lambda^3+12\lambda^2-2\lambda-3}\right], \tag{7}$$

where $f_B^L(\vartheta)$ is the Born approximation of the polarization potential α/r^4 for $\lambda>L$ [31], and N_k is an overall size-fitting parameter. Both Eqs. (6) and (7) without the size parameter were originally developed for spherical potentials, and thus their use in the present context is arbitrary. An alternative has been proposed in a paper on N_2 (Ref. [32]) that makes much more use of the known physical properties of the system and its S matrix, but so far is restricted to homonuclear systems. The Thompson correction in the above equations helps to cover the steep descent at small angles. In the present paper, we restricted the size of $|\beta_\lambda|<1$, i.e., we used the conventions of inelastic phase-shift fitting. In order to obtain the smooth fits, manual adjustments of the initial fitting parameters and L are used, and this procedure is continued till a consistent set of extrapolations over all impact energies (compare Fig. 5 below) and a smooth behavior of the integrated (Q_I) and momentum transfer (Q_M) cross sections (compare Fig. 9 below) are found. Then Q_M at intermediate to high energies is mainly determined by the high angle extrapolation, and Q_I is dominated by the low angle extrapolations where the DCS's are larger. The integrals themselves are obtained by numerical integration under the fits. The fitting coefficients can be obtained from the authors in form of a table or ASCII file.

Note that Eq. (6) should be considered only as a numerical help for manual extrapolations. However, because the extrapolations derived here are guided by a semi-rigorous theoretical frame, we estimate that the numerical error arising from the extrapolation is relatively small, about $\frac{1}{2}-\frac{1}{3}$ of their relative contributions to the integrals. The contributions are listed in the tables below. This error estimate is more conservative than that of Ref. [19], which presumed 10% for Q_I and 5% for Q_M in a similar fitting formula for H_2 observations.

III. THEORETICAL MODEL

We employed a close-coupling method within the fixed-nuclei approximation. Details of the method can be found in Ref. [12]. Hence only a short summary of general aspects of the theory necessary for later discussions is furnished here. However, several important approximations were adopted in our model that realize general improvements over the treatments in earlier studies, and these are separately summarized with some comments on their validity. All calculations were performed in a body-fixed reference frame with the z axis along the molecular axis and the internuclear distance fixed at their equilibrium values. The fixed-nuclei approximation implies an adiabatic treatment of rotational motion.

(A) Molecular states: The molecular electronic states and corresponding wave functions of the target molecular system were determined by two different approaches, namely, (i) the MC-SCF method, and (ii) an *ab initio* SCF method. Both treatments are based on a Gaussian-type basis set [33]. The level of precision of the present Hartree-Fock electronic states is considered to be near the Hartree-Fock limit, and is comparable to or better than those previously determined.

(B) Interaction potentials: The interaction potentials are divided into three parts, namely, static, exchange and correlation polarization potentials,

$$V=V^{\rm st}+V^{\rm ex}+V^{\rm cor}. \tag{8}$$

TABLE I. Total energy and molecular constants. All quantities are in atomic units.

Item		SCF	MC-SCF	Morrison[a] and Hay	Gianturco *et al.*
Total energy	E	−187.7014	−187.6979	−187.68304	
Internuclear distance	R_{co}	2.191 69	2.1922	2.1944	2.1944
Quadrupole moment	Θ_{zz}	−3.802	−3.815	−3.837	−4.0
Spherical polarizability	α_0	17.63	15.76–17.51	15.76	17.9
Nonspherical polarizability	α_2	8.80	8.77	8.06	9.19
Ionization potential	I	0.5060	0.5061	0.5068	-

[a]From M. A. Morrison and P. J. Hay, Phys. Rev. A **20**, 740 (1979).

(i) For the static potential V^{st}, we adopted the formula

$$V^{st}=-\int \frac{\rho(\mathbf{r}')}{|\mathbf{r}-\mathbf{r}'|}\,d\mathbf{r}', \tag{9}$$

where $\rho(\mathbf{r})$ describes the electronic and nuclear charge densities and is obtained from the above molecular electronic wave functions.

(ii) For the exchange potential V^{ex}, we used the Hara-type free-electron-gas model [34], viz.

$$V^{ex}(\mathbf{r})=-\frac{2}{\pi}k_F(\mathbf{r})\left(\frac{1}{2}+\frac{1-\eta^2}{4\eta}\ln\left|\frac{1+\eta}{1-\eta}\right|\right), \tag{10}$$

where

$$\eta(\mathbf{r})=K(\mathbf{r})/k_F(\mathbf{r}), \tag{11}$$

$$K(\mathbf{r})=(k^2+2I+k_F^2)^{1/2}, \tag{12}$$

$$k_F(\mathbf{r})=[3\pi^2\rho_e(\mathbf{r})]^{1/3}; \tag{13}$$

in Eq. (12), I is the ionization potential of the molecule. An earlier study by Collins and Morrison [8] demonstrated that the Hara potential is sufficiently accurate for the present problem.

(iii) The difficulty in describing the correlation-polarization potential rigorously is well known. For the correlation-polarization potential, we adopted the parameter-free free-electron gas-type model of Padial and Norcross [35] for small to intermediate separation regions. For a larger separation, this potential should smoothly connect to the long-range polarization potential which can be described as

$$V^{pol}(\mathbf{r})=-\frac{\alpha_0}{2r^4}-\frac{\alpha_2}{2r^4}P_2(\cos\vartheta), \tag{14}$$

where ϑ is the scattering angle measured in the body-fixed frame, and α_0 and α_2 are defined as

$$\alpha_0=\tfrac{1}{3}(\alpha_\parallel+2\alpha_\perp), \tag{15}$$

$$\alpha_2=\tfrac{2}{3}(\alpha_\parallel-\alpha_\perp). \tag{16}$$

In Eqs. (15) and (16), $\alpha_\parallel$ and $\alpha_\perp$ are the polarizabilities parallel and perpendicular to the molecular axis, respectively.

With the interaction potentials described above, we carried out the scattering calculation by using two sets of close-coupling schemes, namely, (i) a static potential determined by the MC-SCF wave functions, and (ii) a potential derived from the *ab initio* SCF wave function. Some parameters of the exchange and polarization potentials in these two treatments differ slightly since they were determined separately, and, hence, slightly different differential cross sections were observed, particularly in the low-energy region [36]. The values for the polarizabilities along with other quantities used for the SCF wave function can be found in Ref. [12], and all of the parameters used to evaluate the potentials are summarized in Table I. Figure 4 illustrates our correlation potential. Some test calculations within the MC-SCF wave function were performed in order to pin down the origin of the differences in two calculations by artificially changing the parameters for exchange and polarization potentials as described below. The second-order coupled equations were solved numerically by using the Numerov method [37]. We examined the convergence of the DCS's in terms of the number of partial waves to be included in the expansions, and found that in the cross section calculation, it is sufficient to include up to 30 partial waves for convergence to within less than 0.1%. However the highest partial waves included for each symmetry extended up to 40–70 with Σ_g requiring the largest values. Ten symmetries for the total system are included.

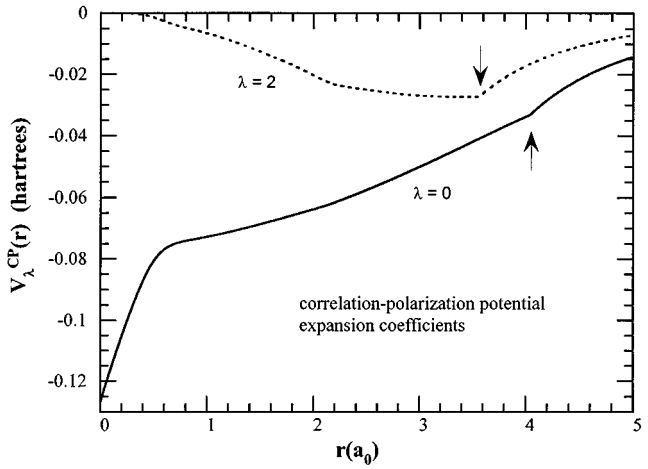

FIG. 4. Plot of the correlation-polarization potential. The arrows indicate where potentials have been matched. Note that V_λ^{CP} is defined in Eq. (11) of Ref. [12].

TABLE II. Elastic DCS's in $Å^2\ sr^{-1}$, and integrated cross sections Q_I and Q_M in $Å^2$. L (%) and R (%) are the percent-contributions of the low- and high-angle extrapolations.

Angle (deg)	1.5 eV	2 eV	3 eV	3.8 eV	4 eV	5 eV	6 eV	6.5 eV	7 eV
20	0.958	0.7505	0.716	1.3536	1.3537	0.5824	0.6823	0.8599	0.8828
30	0.762	0.5472	0.4868	0.8831	1.0269	0.7486	0.773	0.8236	0.8313
40	0.541	0.3896	0.3069	0.6294	0.777	0.8076	0.8244	0.9132	0.9039
50	0.405	0.2455	0.3118	0.5897	0.6857	0.8994	0.8383	0.9286	0.9391
60	0.3289	0.2368	0.3386	0.5715	0.6472	0.8079	0.8373	0.895	0.8025
70	0.2957	0.2489	0.3779	0.5367	0.5834	0.7272	0.7644	0.6978	0.7558
80	0.27	0.2765	0.3876	0.5539	0.5595	0.6026	0.6422	0.6616	0.6258
90	0.2405	0.2845	0.3937	0.5739	0.5037	0.4794	0.5258	0.53	0.5273
100	0.308	0.3021	0.395	0.5096	0.4431	0.391	0.4518	0.4252	0.4333
110	0.304	0.3276	0.438	0.5187	0.4217	0.2647	0.3476	0.339	0.3766
120	0.3567	0.3776	0.483	0.5280	0.4258	0.2523	0.3136	0.3201	0.3798
130	0.365	0.3992	0.5173	0.5475	0.4803	0.2853	0.3798	0.352	0.3724
Q_I	5.04	4.62	5.77	8.25	8.16	6.85	7.59	7.8	7.87
L (%)	8.9	9.3	8	9.4	8.9	4	4.1	5.3	6.2
R (%)	19.1	21.9	23	20.2	19.4	14.5	16.93	15.8	14.8
Q_M	4.48	4.53	5.96	7.69	7.22	5.66	6.69	6.56	6.56
L (%)	0.3	0.3	0.12	0.3	0.3	0.1	0.1	0.2	0.2
R (%)	39.4	40.8	40.7	39.8	40.6	32.4	35.7	34.76	32.7

angle	8 eV	9 eV	10 eV	15 eV	20 eV	30 eV	60 eV	100 eV
15				5.089	7.183	11.52	10.843	7.7149
20	1.1594	1.4958	2.2977	3.843	5.6871	8.731	5.671	3.7543
30	1.002	1.1588	1.5342	2.718	3.2623	3.154	1.786	0.995
40	0.964	1.087	1.2136	1.7789	1.8542	1.4363	0.6597	0.3969
50	0.8542	0.9487	0.9926	1.1756	1.2248	0.743	0.3412	0.2026
60	0.7214	0.8375	0.743	0.7997	0.7475	0.4678	0.1683	0.1502
70	0.6755	0.6622	0.626	0.5777	0.4324	0.306	0.1109	0.1124
80	0.6761	0.5799	0.5468	0.4471	0.3516	0.1896	0.0936	0.084
90	0.5343	0.5394	0.4856	0.3596	0.3041	0.1882	0.0911	0.0697
100	0.4596	0.4811	0.4478	0.3673	0.3071	0.2391	0.0812	0.0754
110	0.4263	0.4381	0.4319	0.4046	0.3887	0.2536	0.1175	0.088
120	0.4058	0.4816	0.5304	0.5445	0.5493	0.3195	0.1805	0.1076
130	0.5183	0.6006	0.7077	0.7832	0.6738	0.4441	0.2748	0.1373
Q	8.99	10.06	11.4	13.79	14.59	15.01	11.04	8.1
L (%)	7.9	8.3	13.1	9.5	13.7	28	42	49
R (%)	20	23.4	23.9	24.7	21	15.2	12.5	10.2
Q_M	8.07	9.24	9.94	11.19	10.17	7.51	4.15	2.65
L (%)	0.2	0.4	0.4	0.2	0.3	0.9	1.5	1.9
R (%)	42.7	47.3	50.8	56.6	56.2	57.9	61.8	58.2

IV. RESULTS

We first discuss the experimental results in some depth and then closely compare experiment and theory, as well as the present two theories.

A. Experimental elastic DCS's and their extrapolation

The absolute elastic DCS's are listed in the upper part of Table II and shown in Fig. 5 together with our extrapolations. The set at 3.8 eV in Table II was obtained differently by covering the region from 2.5 to 5 eV in a series of excitation measurements and normalizing their relative data to the 4-eV DCS. Where comparable measurements exist, our DCS's are in excellent agreement in overall shape with previous publications (see also Fig. 6). Register, Nishimura, and Trajmar [4] pointed out earlier that Shyn, Sharp, and Canguen [3] attempted to achieve a single-point normalization (at 60° using a 10-eV DCS as the reference) over all energies and, consequently, the results of Ref. [3] are sys-

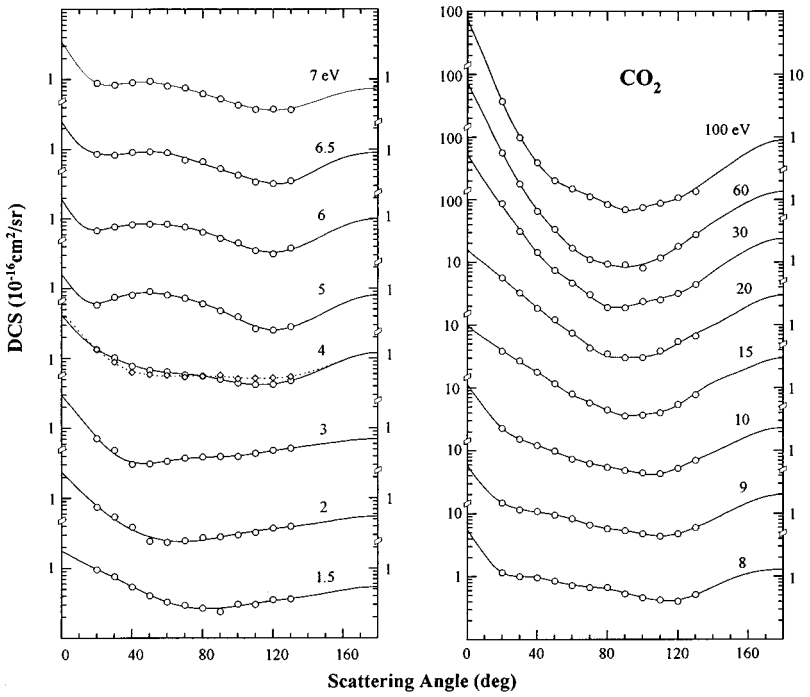

FIG. 5. Elastic DCS and extrapolations. The broken line shows the 3.8-eV set.

tematically higher and more forward peaked. In view of this comment, we have adjusted the relative size of their DCS independently for each energy (the normalization factors are indicated in the labels of the figure). The data for the small energy step at 5, 6, 6.5, and 7 eV were included to confirm the different shape of the 5-eV DCS as a systematic transition from 5 to 7 eV.

Several features dominate in our experimental DCS's: (a) The resonance in the neighborhood of 3.8 eV is usually identified as a $^2\Pi_u$ shape resonance, and clearly differs in size and shape from the nearby smooth background. (b) The general shapes of the DCS's split into two patterns, those below and above the resonance at 3.8 eV. In particular, the pattern at low energies has a minimum that shifts toward larger angles with decreasing energies and its right hand sections form nearly straight lines. Theory agrees with these trends (see below). (c) The general shapes show different features, again, above 5 eV. The experimental data may be related to two patterns: either to the standard pattern observed in many other gases (e.g., CH_4 and H_2 at 5 eV) where the DCS's sharply rise at very small angles, or second, to the pattern of certain linear molecules (e.g., O_2, N_2, NO, and CO; see Ref. [38]) where the elastic DCS's of low impact energies continue to drop down for angles approaching zero, and theoretical confirmation exists for N_2 [32]. We have taken the first view in our extrapolations only because an extrapolation to a minimum in the 5–9 eV energy region without doing the same below resonance would be very subjective. The contribution to the integrated momentum transfer Q_M from the left extrapolation is minimal ($<0.3\%$). For a horizontal extrapolation, the contribution to the integrated cross sections would change from the value that can be read off the percentage row in Table II to 0.222 (5 eV), 0.258 (6 eV), 0.326 (6.5 eV), 0.334 (7 eV), 0.439 (8 eV), and 0.566 (9 eV). Contributions from an extrapolation to a minimum would be approximately half of these values. (d) The 100-eV DCS shows a structure that was also observed in Ref. [3] and again is reproduced by the present theory (see below). At these energies we enter a region where simple independent atom model calculations [6,11,39] represent the data in the observed angular region rather well, and contain at least some of the structure. It may be due to ''interference between single scattering centers'' [39,40] in multiple scattering within a single molecule [41].

A three-dimensional plot of the complete set of DCS's over all energies and angles is presented in Fig. 7, and clearly shows that the peak observed at 3.8 eV, 20°, does not form a constant ridge over all angles. Direct scattering may interfere with the $^2\Pi_u$ shape resonance at 3.8 eV or several types of resonances may be present, as recently proposed by Cartwright and Trajmar [42].

B. Comparison of theory and experiment

Comparisons with theoretical differential DCS's are shown in Fig. 8. The theoretical results are all based on close-coupling calculations in the fixed-nuclei approximation. For the discussion we divide the scattering energy into three regions designated as I, II and III, respectively.

Region I (1.5–4 eV): The angular distributions obtained with electrons of 1.5–4 eV incidence energy are displayed in the first plot of Fig. 8. The experimental data show a dip around 40° at 3 eV. The dip moves toward a larger scattering angle of nearly 90° as the energy decreases to 1.5 eV. But at 4 eV, neither a significant structure nor a dip can be seen except for a remnant of the shoulder at 60° from the lower-energy data. The theoretical result based on the MC-SCF wave function seems to reproduce the angular dependence of the measurements reasonably well, although its magnitude is somewhat larger at scattering angles below 60°. The result based on the SCF wave function shows a shoulder around 60° that is similar to the structure seen in the measurements at energies between 5 and 7 eV (see below). The result of the MC-SCF wave function shows a weak change of the slope in

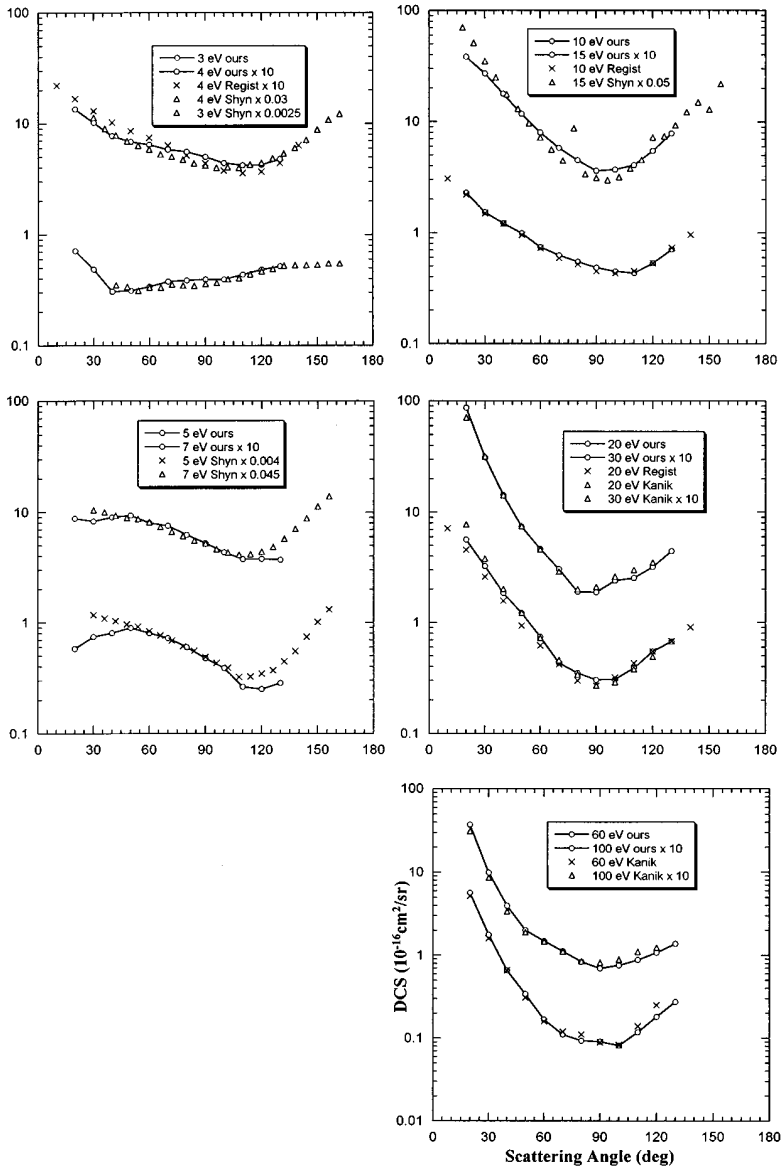

FIG. 6. Comparison with other experimental DCS measurements.

the DCS in the same region that is not recognizable in the figure but is consistent with the SCF wave function. Except for this shoulder region, the two theoretical treatments at 1.5 and 2 eV agree well in magnitude. The primary cause of the difference in the two theories may be ascribed to the treatment of the exchange and polarization potentials and, to a certain degree, target electronic wave functions. Some test calculations were carried out by artificially varying the parameters of the exchange and polarization potentials employed in the MC-SCF wave function to identify the origin of the difference. When the exchange parameter of Ref. [36] is increased by 15–20 %, a structure develops around 60°. The effect appears more strongly in this energy region, but is less conspicuous at different energies. On the other hand, when the spherical polarizability α_0 and the correlation potential were increased by 20%, the magnitude of the DCS near 0° was increased by about the same amount, but no structure developed in the 60° region. Thus the slight changes in these portions of the theory may have produced the differences in the angular dependencies of the two calculations, particularly at around 60°. Agreement between the present results and those of Ref. [13] at 4 eV is poor in shape and magnitude, mainly due to a different treatment of all potentials.

Region II (5–7 eV): The angular distributions for 5–7 eV are displayed in the second plot of Fig. 8. A shoulder appears in all energies of this region around the scattering angle of 60°. At 5 eV, the shoulder is most conspicuous, and becomes a prominent peak at 50°. The experimental DCS's drop as the scattering angle decreases from the peak position. The calculation by the SCF wave function, however, only shows a small change of slope at about 70°. The theoretical DCS decreases monotonically with increasing scattering angles, and is followed by a minimum around 110°–120°. Except for the region of angles below the shoulder, the present theory generally agrees with the measurement in magnitude and shape. Another theoretical result based on the MC-SCF wave function shows an even weaker change of slope near 60°, and slightly larger magnitudes of DCS's as compared with the SCF wave function. A similar small-angle behavior of the DCS was found for N_2 and other polyatomic molecules, and discussed in Ref. [32].

The polarization potentials used here may be responsible for these discrepancies between theory and experiment, in

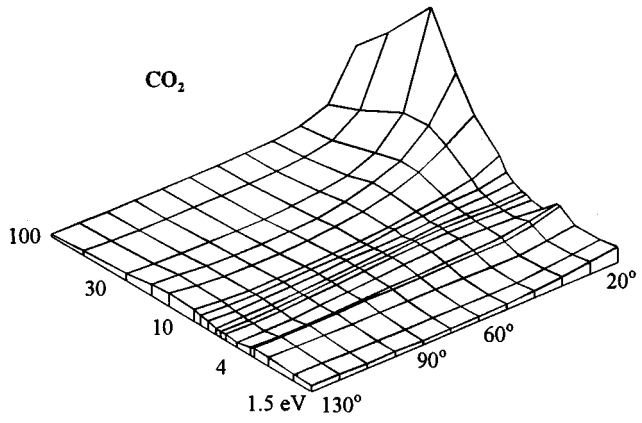

FIG. 7. Three-dimensional plot of the elastic DCS. The vertical scale is linear.

addition to the different target electronic wave functions. The lowering of the forward peak may be ascribed, at least partly, to interference or partial cancellation between the long-range parts of the electrostatic and the polarization interactions. In fact, the quadrupole moment and the polarizability have different signs, so that they contribute to the interaction in opposite ways. To take account of this interference accurately, we need a much more elaborate treatment of the polarization effect, and plan a study along this line in the future.

Region III (10–100 eV): The angular distributions for the energy above 7 eV are shown in the third and fourth plots of Fig. 8. The measured cross sections have a conventional shape, that is, a large magnitude at forward-scattering angles, reaching a minimum around 90° that is followed by slight increases at still larger scattering angles. DCS's at angles below 30° begin to increase sharply as the energy increases and, accordingly, the minimum becomes more accentuated. This minimum moves toward smaller angles from 120° at 10 eV to less than 90° at 100 eV. The theoretical calculations are in excellent agreement with the measurements in these energy and angle regions. Details of the theoretical results and the comparison with previous theoretical and experimental studies in this energy region were reported earlier in Ref. [12].

The calculations by Gianturco and Stoecklin [13] appeared after completion of our measurements. They covered the energy range from 0.02 to 100 eV, were based on a single center expansion formalism, and used a separable exchange representation with some 70 exchange basis functions. The entries in our comparisons plots have been read off their plots (linear DCS scale) and therefore might be somewhat inaccurate at higher impact energies. Generally, the two theories are found to be in harmony where they overlap.

C. Integrated and momentum-transfer cross section

The upper part of Fig. 9 shows the integrated cross sections Q_I from Table II. The only comparable experimental

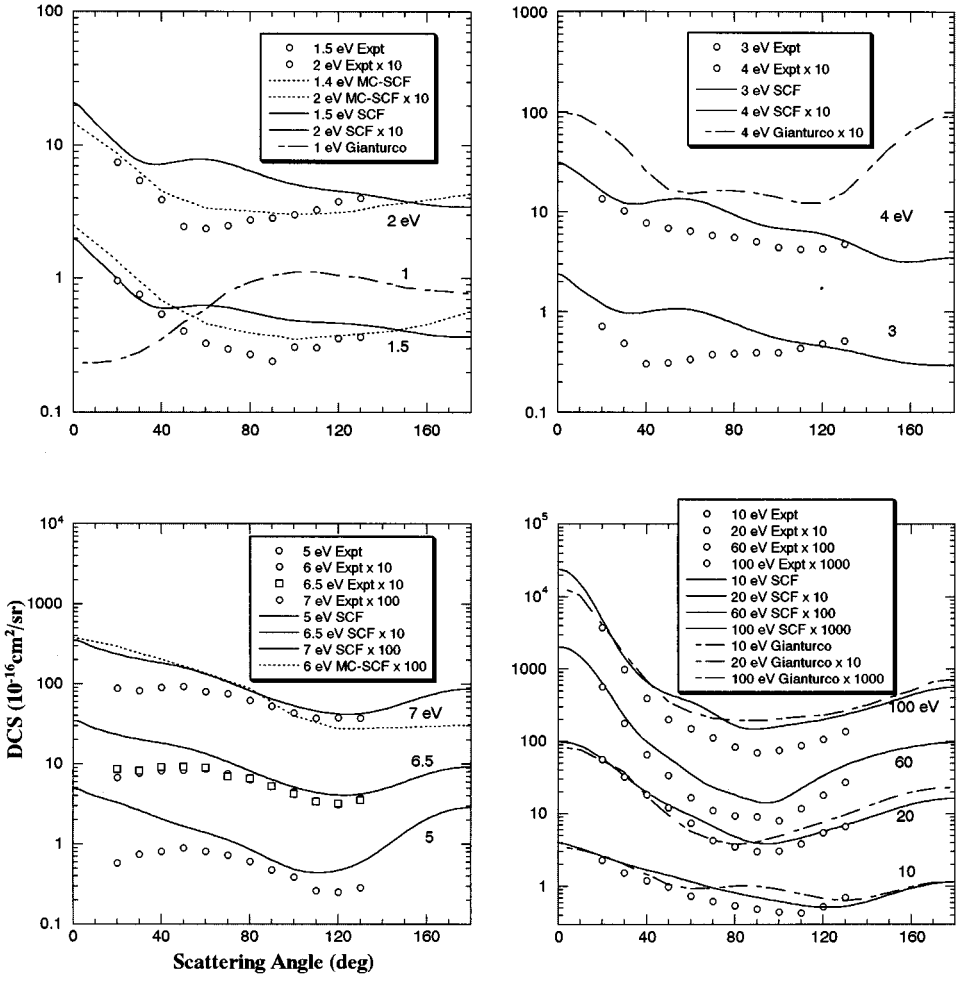

FIG. 8. Comparison of experimental values with various theoretical differential DCS's.

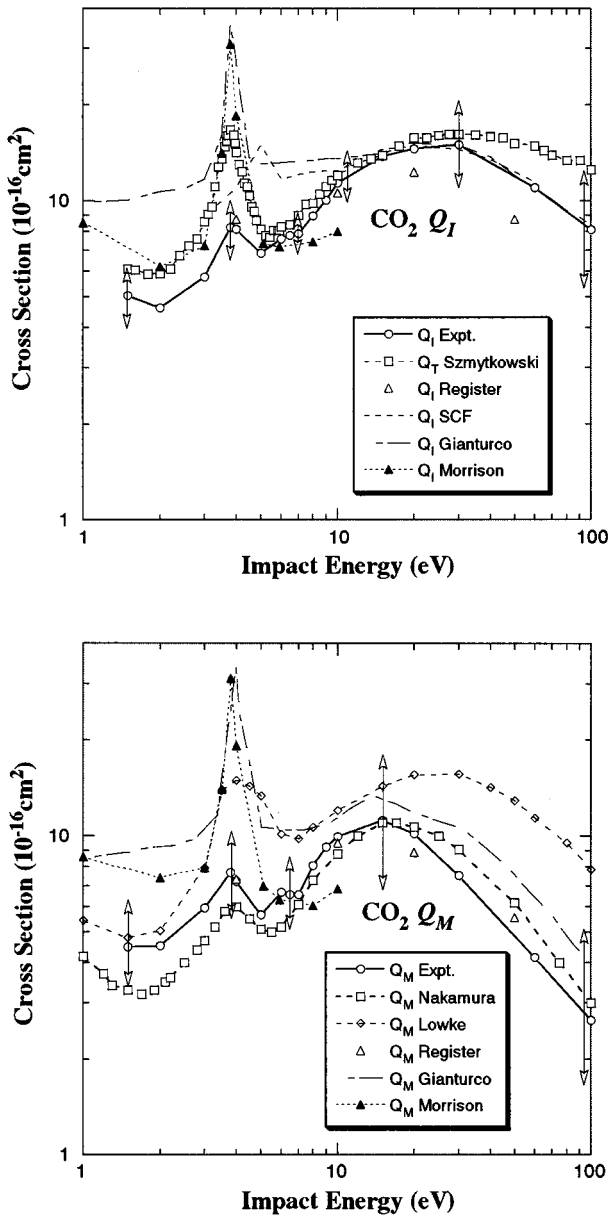

FIG. 9. Integral and momentum-transfer cross sections. The arrows indicate 50% of the contributions from the extrapolations.

data are the four entries of Ref. [4]. They extrapolated their DCS's at 20 and 50 eV at small angles less steeply than we do, so that their Q_I is lower than ours at those energies. In the figure we also include the total scattering cross sections Q_T measured by Szmytkowski *et al.* [43]. They contain a large contribution of vibrational excitation at lower energies, and electronic excitation at higher energies. Thus they form an upper bound for Q_I. As is seen in the figure, the present measurement and extrapolation gives values of Q_I consistent with Q_T of Szmytkowski *et al.* The latter authors attributed the differences to the older measurements of Q_T [44–46] to a better energy resolution. The large peak at the resonance was confirmed in Ref. [47]. In the figure we also include the results of three theoretical calculations: the present SCF wave function and the calculation by Gianturco and Stoecklin [13], together with that of Morrison and co-workers [8]. The former two calculations reproduce the present measurement at and above 10 eV reasonably well, but give rather large cross sections below 10 eV. The discrepancy between the theory and experiment may be ascribed again to the inadequacy of the polarization potential. Actually Gianturco and Stoecklin, as well as our own test with the MC-SCF wave function, demonstrated that DCS's in the lower-energy region are significantly sensitive to the polarization interaction. Finally, the differences between the two theoretical results in the lower-energy region probably arise from a different treatment of the exchange interaction and the target wave functions [48]. We will report a more complete study of the total and momentum transfer cross sections elsewhere.

The momentum-transfer cross sections Q_M are presented in the lower section of Fig. 9 together with calculation from Ref. [8] and two evaluations from swarm-experiments (quoted in Ref. [7]). Fits to the Boltzmann equation are used to derive Q_M from electron swarm data, and thus their determinations are indirect when compared with ours. As shown in Table II, the high-angle extrapolation contributes significantly to Q_M (at high energies even more than 50%). Nevertheless, even if we would extend our low-energy extrapolations horizontally, we would not be able to achieve Nakamura's low values in the energy region below 4 eV. Also, we tried very much to find fits that reproduce the valley of the two swarm experiments near 6.5 eV, to no avail. Any definite conclusion about the comparison between swarm measurements and beam-type experiments should be reserved until more data are available at the large scattering angles.

V. CONCLUSION

We have studied experimentally the elastic processes in collisions of electrons with a CO_2 molecule at collision energies from 1.5 to 100 eV, and scattering angles from 20° to 130°. Theoretical calculations based on a close coupling nicely reproduce most of the measurements. For small energies below 4 eV, the present theoretical results based on the MC-SCF method for the static potential agree well with the present measurement, but fail to reproduce the shoulder structure near 60° in the scattering energies 3–7 eV. Above this energy, the present SCF method and experiments are found to be in excellent harmony at all scattering angles.

Many recent investigations on carbon dioxide have shown a trend to concentrate on the more interesting vibrational excitation processes of this molecule. In this paper we tried to fill a void in the basic knowledge about the behavior of carbon dioxide in collisions with slow electrons. We hope the recent theoretical efforts will be continued so that a full set of DCS's can be found at all the energies, including the region near the 3.8-eV resonance.

ACKNOWLEDGMENTS

This work was supported in part by the U.S. Department of Energy, Office of Basic Energy Sciences through Rice University (M.K.). M.K. would like to thank Dr. N. F. Lane for useful discussions in the early stage of the study.

[1] J. H. Black and A. Dalgarno, Astrophys. J. **34**, 405 (1977).
[2] Y. Itikawa and M. Shimizu, Bull. Inst. Space Aeron. Sci. **7**, 64 (1971).
[3] T. W. Shyn, W. E. Sharp, and G. R. Carignan, Phys. Rev. A **17**, 1855 (1978).
[4] D. F. Register, H. Nishimura, and S. Trajmar, J. Phys. B **13**, 1651 (1980).
[5] I. Kanik, D. C. McCollum, and J. C. Nickel, J. Phys. B **22**, 1225 (1989).
[6] I. Iga, J. C. Nogueira, and M.-T. Lee, J. Phys. B **17**, L185 (1984).
[7] Y. Nakamura, Aust. J. Phys. **48**, 357 (1995).
[8] M. A. Morrison, N. F. Lane, and L. A. Collins, Phys. Rev. A **15**, 2186 (1977); see also L. A. Collins and M. A. Morrison, *ibid.* **25**, 1764 (1982).
[9] R. R. Lucchese and V. McKoy, Phys. Rev. A **25**, 1963 (1982).
[10] D. Thirumalai, K. Onda, and D. G. Truhlar, J. Chem. Phys. **74**, 6792 (1981); K. Onda and D. G. Truhlar, J. Phys. B **12**, 283 (1979).
[11] L. F. Botelho, L. C. G. Freitas, M-T. Lee, A. Jain, and S. S. Tayal, J. Phys. B **17**, L641 (1984).
[12] M. Takekawa and Y. Itikawa, J. Phys. B **29**, 4227 (1996); see also M. Takekawa, Master's thesis, Tokyo University, 1996 (in Japanese).
[13] F. A. Gianturco and T. Stoecklin, J. Phys. B **29**, 3933 (1996).
[14] F. A. Gianturco and R. R. Lucchese, J. Phys. B **29**, 3955 (1996).
[15] J. C. Nickel, P. W. Zetner, G. Shen, and S. Trajmar, J. Phys. E **22**, 730 (1989).
[16] S. K. Srivastava, A. Chutjian, and S. Trajmar, J. Chem. Phys. **63**, 2659 (1975).
[17] R. T. Brinkman and S. Trajmar, J. Phys. E **14**, 245 (1981).
[18] S. Trajmar and D. F. Register, in *Electron-Molecule Collisions*, edited by I. Shimamura and K. Takayanagi (Plenum, New York, 1984), Chap. 6, p. 468.
[19] M. A. Khakoo and S. Trajmar, Phys. Rev. A **34**, 138 (1986).
[20] M. J. Brunger, S. J. Buckman, D. S. Newman, and D. T. Alle, J. Phys. B **24**, 1435 (1991).
[21] D. T. Alle, R. J. Gulley, S. J. Buckman, and M. J. Brunger, J. Phys. B **25**, 1533 (1992).
[22] M. A. Khakoo, T. Jayaweera, S. Wang, and S. Trajmar, J. Phys. B **26**, 4845 (1993).
[23] A. Roth, *Vacuum Technology* (North-Holland, Amsterdam, 1983), p. 447.
[24] *Atom und Molekular Physik*, edited by A. Eucken, Landolt-Bornstein, Vol. I, Pt. 1 (Springer Verlag, Berlin, 1950), pp. 325 and 370.
[25] R. C. Reid, J. M. Prausnitz, and B. E. Poling, *The Properties of Gases and Liquids* (McGraw-Hill, New York, 1986), Chap. 9 and Appendixes A and B.
[26] D. R. Olander and V. Kruger, J. Appl. Phys. **41**, 2769 (1970).
[27] S. J. Buckman, R. J. Gulley, M. Moghbelalhossein, and S. J. Bennett, Meas. Sci. Technol. **4**, 1143 (1993).
[28] L. Boesten, Rev. Sci. Instrum. **59**, 233 (1988).
[29] J. N. H. Brunt, G. King, and F. H. Read, J. Phys. B **10**, 433 (1977).
[30] L. Boesten and H. Tanaka, At. Data Nucl. Data Tables **52**, 25 (1992).
[31] D. G. Thompson, Proc. R. Soc. London, Ser. A **294**, 160 (1966).
[32] W. Sun, M. A. Morrison, W. A. Isaacs, W. K. Trail, D. T. Alle, R. J. Gulley, M. J. Brennan, and S. J. Buckman, Phys. Rev. A **52**, 1229 (1995).
[33] G. C. Lie and E. Clementi, J. Chem. Phys. **60**, 1275 (1974).
[34] S. Hara, J. Phys. Soc. Jpn. **22**, 710 (1967).
[35] N. T. Padial and D. W. Norcross, Phys. Rev. A **29**, 1742 (1984).
[36] The MC-SCF wave function was developed to study vibrational excitation in CO_2 molecules, and, therefore, some parameters in the exchange and polarization potentials were adjusted for better agreement with experiments in the vibrational excitation cross sections.
[37] B. R. Johnson, J. Comput. Phys. **13**, 445 (1973).
[38] J. P. Sullivan, J. C. Gibson, R. J. Gulley, and S. J. Buckman, J. Phys. B **28**, 4319 (1995).
[39] A. Jain and S. S. Tayal, J. Phys. B **15**, L867 (1982).
[40] S. Hayashi and K. Kuchitsu, J. Phys. Soc. Jpn. **41**, 1724 (1976); Chem. Phys. Lett. **41**, 575 (1976).
[41] B. H. Choi, R. T. Poe, J. C. Sun, and Shan Yueh, Phys. Rev. A **19**, 116 (1979).
[42] D. C. Cartwright and S. Trajmar, J. Phys. B **29**, 1549 (1996).
[43] C. Szmytkowski, A. Zecca, G. Karwasz, S. Oss, G. K. Macia, Marinkokovic', R. S. Brusa, and R. Grisenti, J. Phys. B **20**, 5817 (1987).
[44] C. K. Kwan, Y. F. Hsieh, W. E. Kauppila, S. J. Smith, T. S. Stein, M. N. Uddin, and M. S. Dababneh, Phys. Rev. A **27**, 1328 (1983).
[45] K. R. Hoffman, M. S. Dababneh, Y. F. Hsieh, W. E. Kauppila, V. Pol, J. H. Smith, and T. S. Stein, Phys. Rev. A **25**, 1393 (1982).
[46] O. Sueoka and S. Mori, J. Phys. Soc. Jpn. **53**, 2491 (1984).
[47] S. J. Buckman, M. T. Elford, and D. S. Newman, J. Phys. B **20**, 5175 (1987).
[48] N. F. Lane, Rev. Mod. Phys. **52**, 29 (1980).